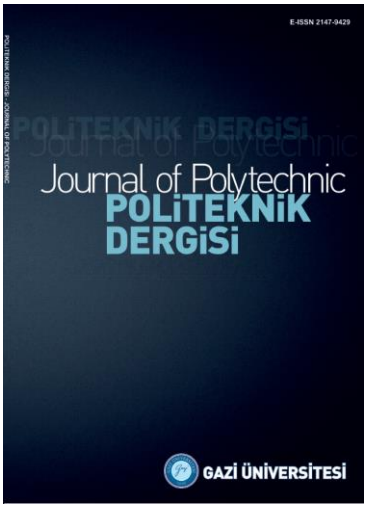

POLİTEKNİK DERGİSİ

JOURNAL of POLYTECHNIC

ISSN: 1302-0900 (PRINT), ISSN: 2147-9429 (ONLINE)
URL: http://dergipark.gov.tr/politeknik

Estimation of entropy generation for Ag-MgO/water hybrid nanofluid flow through rectangular minichannel by using artificial neural network

Dikdörtgen kesitli minikanalda Ag-MgO/su hibrit nanoakışkan akışının entropi üretiminin yapay sinir ağları kullanılarak tahmin edilmesi

***Yazar(lar) (Author(s))**: Cuneyt UYSAL[1], Mehmet Erdi KORKMAZ[2]*

ORCID[1]: 0000-0002-7986-1684

ORCID[2]: 0000-0002-0481-6002

Bu makaleye şu şekilde atıfta bulunabilirsiniz(To cite to this article): Uysal C., Korkmaz M. E., "Estimation of entropy generation for Ag-MgO/water hybrid nanofluid flow through rectangular minichannel by using artificial neural network", ***Politeknik Dergisi***, 22(1): 41-51, (2019).

Erişim linki (To link to this article): http://dergipark.gov.tr/politeknik/archive

DOI: **10.2339/politeknik.417756**

Estimation of Entropy Generation for Ag-MgO/Water Hybrid Nanofluid Flow through Rectangular Minichannel by Using Artificial Neural Network

Araştırma Makalesi / Research Article

Cuneyt UYSAL[1*], Mehmet Erdi KORKMAZ[2]

[1]Automotive Technologies Program, TOBB Vocational School of Technical Sciences, Karabuk University, Turkey.
[2]Mechanical Engineering Department, Faculty of Engineering, Karabuk University, Turkey.

(Geliş/Received : 27.10.2017 ; Kabul/Accepted : 10.04.2018)

ABSTRACT

The convective heat transfer and entropy generation characteristics of Ag-MgO/water hybrid nanofluid flow through rectangular minichannel were numerically investigated. The Reynolds number was in the range of 200 to 2000 and different nanoparticle volume fractions were varied between ϕ = 0.005 and 0.02. In addition, Artificial Neural Network was used to create a model for estimating of entropy generation of Ag-MgO/water hybrid nanofluid flow. As a result, it was found that the convective heat transfer coefficient for ϕ = 0.02 Ag-MgO/water hybrid nanofluid is 21.29% higher than that of pure water, at Re=2000. Total entropy generation of Ag-MgO/water hybrid nanofluid increased with increasing nanoparticle volume fraction. The results obtained by ANN showed good agreement with the numerical results obtained in this study.

Keywords: Artificial neural network, convective heat transfer, entropy generation, hybrid nanofluid.

Dikdörtgen Kesitli Minikanalda Ag-MgO/Su Hibrit Nanoakışkan Akışının Entropi Üretiminin Yapay Sinir Ağları Kullanılarak Tahmin Edilmesi

ÖZ

Dikdörtgen kesitli minikanalda Ag-MgO/su hibrit nanoakışkan akışının taşınımla ısı transferi ve entropi üretimi karakteristikleri sayısal olarak incelenmiştir. Reynolds sayısı 200 ile 2000 aralığındadır ve nanopartikül hacimsel oranı ise ϕ = 0.005 ve 0.02 aralığında değiştirilmiştir. İlave olarak, Ag-MgO/su hibrit nanoakışkan akışının entropi üretiminin tahmin edilmesi için Yapay Sinir Ağları kullanılmıştır. Sonuç olarak, Re = 2000'de, ϕ = 0.02 sahip Ag-MgO/su hibrit nanoakışkanının ısı taşınım katsayısının saf suyunkine kıyasla % 21.29 daha fazla olduğu bulunmuştur. Ag-MgO/su hibrit nanoakışkanının toplam entropi üretimi nanopartikül hacimsel oranının artmasıyla artmaktadır. Yapay sinir ağları ile elde edilen sonuçlar bu çalışmada elde edilen sayısal analizden elde edilen sonuçlar ile iyi bir uyum göstermektedir.

Anahtar Kelimeler: Yapay sinir ağları, taşınımla ısı transferi, entropi üretimi, hibrit nanoakışkanlar.

1. INTRODUCTION

The idea based on solid particle addition to working fluids to enhance their thermophysical properties was firstly proposed by Maxwell in 1881 [1]. However, this idea has not been put into practice because of that solid particles having millimeter-sized caused to aggregation, sedimentation, clogging and abrasion problems in piping systems. In last decade, rapidly developing in nanotechnology made solid particles having nanometer-sized possible. By this means, the "*nanofluid*" concept was developed. The nanofluid term was firstly introduced by Choi and Eastman in 1995 [2] and it was prepared with metallic or non-metallic nanoparticle addition to conventional working fluids such as water, ethylene glycol or lubricants.

**Sorumlu yazar (Corresponding Author)*
e-posta : cuneytuysal@karabuk.edu.tr

In last decade, several studies have been performed on nanofluid to determine their thermophysical properties such as viscosity [3-9] and thermal conductivity coefficient [7-13] and to determine their convective heat transfer [14-23] and fluid flow characteristics [14, 21-23]. The idea for obtaining better heat transfer and fluid flow characteristics compared to individual nanofluids led to developing of hybrid nanofluids. Hybrid nanofluids are prepared either by dispersing dissimilar nanoparticles as individual constituents or by dispersing nanocomposite particles in the base fluid [24]. The determination of thermophysical properties and heat transfer and fluid flow characteristics of hybrid nanofluids became important due to their better properties such as thermophysical properties, chemical stability, physical strength and mechanical resistance compared to individual nanofluids.

A few study have been performed on determination of thermophysical properties and heat transfer and fluid flow characteristics of individual and hybrid nanofluids by using artificial neural network.

Atashrouz et al. [25] developed a hybrid self-organizing polynomial neural network to evaluate viscosity values of nine nanofluids based on water, ethylene glycol and propylene glycol. Their results showed good agreement when compared to theoretical and empirical correlations. High regression coefficient of R=0.9978 was obtained. Longo et al. [26] predicted the dynamic viscosity of oxide nanoparticle suspensions based on water and ethylene glycol with artificial neural network. The model showed good agreement with the experimental data. The mean absolute percentage error was obtained to be 4.15%. Longo et al. [27] used a 3-input and a 4-input artificial neural network model to predict the thermal conductivity coefficient of oxide-water nanofluids. They reported that both models showed good agreement with experimental data. Esfe et al. [28] used artificial neural network in the prediction of viscosity and thermal conductivity of ferromagnetic nanofluids by using input experimental data, which are temperature, diameter of particles and nanoparticle volume fraction. They found that the maximum errors in predicting thermal conductivity and dynamic viscosity are 2% and 2.5%, respectively. Esfe et al. [29] investigated the change of thermal conductivity of Cu/TiO_2-water/ethylene glycol hybrid nanofluid with nanoparticle volume fraction and temperature. They proposed a correlation via artificial neural network by using these data based on experimental results. They reported that proposed correlation showed good agreement with experimental data.

Santra et al. [30] predicted the laminar natural convection of Cu/water nanofluid in a differentially heated square cavity by using Artificial Neural Network. They showed that ANN gives reliable results within the given range of training data. Tafarroj et al. [31] predicted the heat transfer coefficient and Nusselt number of TiO_2/water nanofluid flow through a microchannel heat sink with artificial neural network. They reported that the average relative errors in the prediction of Nusselt number and heat transfer coefficients are 0.3% and 0.2%, respectively. Ghahdarijani et al. [32] experimentally investigated the effect of water based Al_2O_3 and CuO nanofluids on the cooling performance and pressure drop of a jacket reactor. In addition, they used artificial neural networks based on two optimal models via feed-forward back-propagation multilayer perceptron. They obtained good agreement between the results of artificial neural networks and experiments for convective heat transfer and pressure drop. Safikhani et al. [33] investigated the heat transfer coefficient and pressure drop of Al_2O_3/water nanofluid flow through flat tubes by using computational fluid dynamics, artificial neural networks and Non-dominated Sorting Genetic Algorithms. Tomy et al. [34] simulated the silver/water nanofluid flow for flat plate solar collector by using Artificial Neural Networks. They found that the results obtained by using ANN show good agreement with the experimental data with the deviation less than $\pm$ 2%.

To the best knowledge of authors, there is only a study, which is published by Bahiraei and Majd [35], for estimation of entropy generation of nanofluid flow by using artificial neural network. Bahiraei and Maid [35] numerically investigated the entropy generation of Al_2O_3/water nanofluid flow through triangular minichannel for some parameters such as Reynolds number, nanoparticle diameter, nanoparticle volume fraction etc. In addition, an artificial neural network model is created to estimate the entropy generation of Al_2O_3/water nanofluid flow in their study. They reported that the ANN model used in the study predicts the thermal, frictional and total entropy generations rates with mean absolute error (MAE) of 4.36×10^{-7}, 3.36×10^{-9}, 4.33×10^{-7} and with mean square error (MSE) of 2.43×10^{-13}, 2.01×10^{-17}, 2.37×10^{-13}, respectively.

In this study, convective heat transfer and entropy generation of Ag-MgO/water hybrid nanofluid through rectangular minichannel under constant heat flux are numerically investigated. The effects of Reynolds number and nanoparticle volume fraction are evaluated. In addition, an Artificial Neural Network model is created for the estimation of entropy generation. To the best knowledge of authors, this is the first survey for convective heat transfer and entropy generation of Ag-MgO/water hybrid nanofluid and the one of limited studies that uses artificial neural network for entropy generation of nanofluids.

2. MODEL DESCRIPTION and GOVERNING EQUATIONS

The hydraulic diameter of a channel is calculated by using $D_h = 4A_c/P$ formula, where A_c is cross-section area and P is perimeter. If hydraulic diameter obtained for a channel is between 200 μm and 3 mm, the channel is called as minichannel [36]. The geometry considered in this study is a rectangular minichannel having width of 3mm, height of 5 mm and length of 1m.

The flow is modeled as single-phase flow. It is due to that the fluid flow contains infinitesimal solid particles less than 100 nm [37]. Moreover, the flow is considered under three-dimensional, steady-state, incompressible flow conditions. The governing equations can be written with negligible buoyancy effect, viscous dissipation and radiation heat transfer as follows:

$$div(\rho\vec{V}) = 0 \tag{1}$$

$$div(\rho\vec{V}\vec{V}) = -grad\,P + div(\mu\,grad\,\vec{V}) \tag{2}$$

$$div(\rho Cp\vec{V}T) = div(k\,grad\,T) \tag{3}$$

where ρ, Cp, k and μ are the density, specific heat, thermal conductivity coefficient and dynamic viscosity of fluid, respectively. In addition, T and P represent temperature and pressure, respectively.

As can be seen from Eqs. 1-3, the governing equations are including thermophysical properties of working fluid. Therefore, the thermophysical properties should be defined for Ag-MgO/water hybrid nanofluid

2.1. Thermophysical properties of Ag-MgO/water hybrid nanofluid

In this study, Ag-MgO/water hybrid nanofluid with nanoparticle volume fraction ranged between ϕ = 0.005 and 0.02 is used as working fluid. The density and specific heat of Ag-MgO hybrid nanoparticle can be calculated by the following equations, respectively.

$$\rho_{Ag-MgO} = \frac{(\rho_{Ag} W_{Ag}) + (\rho_{MgO} W_{MgO})}{(W_{Ag} + W_{MgO})} \quad (4)$$

$$Cp_{Ag-MgO} = \frac{(Cp_{Ag} W_{Ag}) + (Cp_{MgO} W_{MgO})}{(W_{Ag} + W_{MgO})} \quad (5)$$

where W is weight. For this study, the volumetric fractions of Ag and MgO nanoparticles in the content of Ag-MgO hybrid nanoparticle is assumed to be 50% and 50%, respectively [38]. The weight of each nanoparticle is calculated by using $W = \rho \forall g$ formula (where $\forall$ is volume and g is gravitation) for a defined volume value of nanoparticle.

The density and specific heat of Ag-MgO/water nanofluid is defined by using the following equations, respectively.

$$\rho_{nf} = \phi \rho_{np} + (1-\phi)\rho_{bf} \quad (6)$$

$$Cp_{nf} = \phi Cp_{np} + (1-\phi)Cp_{bf} \quad (7)$$

where ϕ is nanoparticle volume fraction and the *nf*, *np* and *bf* subscripts denote nanofluid, nanoparticle and base fluid, respectively. The thermal conductivity coefficient and dynamic viscosity of Ag-MgO/water hybrid nanofluid is presented by Esfe et al. [38] as an empirical correlation in the function of nanoparticle volume concentration. For this study, these empirical correlations proposed by Esfe et al. [38] are used to calculate thermal conductivity coefficient and dynamic viscosity of Ag-MgO/water hybrid nanofluid.

$$k_{nf} = \left(\frac{0.1747 \times 10^5 + \phi}{0.1747 \times 10^5 - 0.1498 \times 10^6 \phi + 0.1117 \times 10^7 \phi^2 + 0.1997 \times 10^8 \phi^3} \right) k_{bf} \quad (8)$$

$$\mu_{nf} = \left(1 + 32.795\phi - 7214\phi^2 + 714600\phi^3 - 0.1941 \times 10^8 \phi^4\right) \mu_{bf} \quad (9)$$

The experiments to obtain empirical correlations mentioned above are realized for nanoparticle volume fraction range of $0 \le \phi \le 0.02$ for Ag-MgO/water hybrid nanofluid by Esfe et al. [38]. Therefore, these correlations are valid in the range of $0 \le \phi \le 0.02$.

2.2. Boundary conditions

At the minichannel inlet, the uniform temperature and velocity profiles are adopted. The inlet temperature of Ag-MgO/water hybrid nanofluid is assumed to be 303 K; whereas, the inlet velocity of Ag-MgO/water hybrid nanofluid is calculated by using Reynolds number formula, which is $V = (\mu Re)/(\rho D_h)$, for a defined Reynolds number. In this study, the Reynolds number is in the range of 200 $\le$ *Re* $\le$ 2000. At the minichannel outlet, the pressure outlet boundary condition is applied. At the minichannel walls, no-slip condition is valid. Constant heat flux of 100 W/m^2 is applied to bottom wall of minichannel. The remained walls of minichannel are assumed to be insulated.

3. ENTROPY GENERATION

Entropy is defined as the measure of molecular disorder and randomness. Entropy generation analysis informs the designer about the irreversibility due to flow friction and heat transfer through a finite temperature difference, mixing, chemical reactions etc. [39]. For internal flow, the entropy generation per unit length can be expressed as follows [39].

$$\dot{S}'_{gen,total} = \dot{S}'_{gen,heat\ transfer} + \dot{S}'_{gen,fluid\ friction} \quad (10)$$

where the first term on right side of Eqs. 10 is entropy generation due to heat transfer per unit length and it is written as follows:

$$\dot{S}'_{gen,heat\ transfer} = \frac{q''^2 \pi D_h^{\ 2}}{k T_b^{\ 2} Nu} \quad (11)$$

where q'' is heat flux. T_b is bulk temperature and it is defined as $T_b = (T_{in} + T_{out})/2$. The Nusselt number (Nu) is calculated by using following equation.

$$Nu = \frac{h D_h}{k} \quad (12)$$

where h is the convective heat transfer coefficient and it is given by following equation:

$$h = \frac{1}{A}\int_A \frac{q''}{(T_w - T_b)} dA \quad (13)$$

where T_w and T_b are wall temperature and bulk temperature, respectively.

The second term on right side of Eqs. 10 is entropy generation due to fluid friction per unit length and it is expressed as follows:

$$\dot{S}'_{gen,fluid\ friction} = \frac{8\dot{m}^3}{\pi^2 \rho^2 T_b} \frac{f}{D^5} \quad (14)$$

where $\dot{m}$ is the mass flow rate and it is defined as $\dot{m} = \rho A V$. f is the Darcy friction factor and it can be calculated with following equation:

$$f = 2\frac{D}{L}\frac{\Delta P}{\rho V^2} \quad (15)$$

where ΔP is pressure drop.

By this way, Eqs. 10 is rewritten as follows:

$$\dot{S}'_{gen,total} = \frac{q''^2 \pi D_h^2}{k T_b^2 Nu} + \frac{8\dot{m}^3}{\pi^2 \rho^2 T_b} \frac{f}{D_h^5} \quad (16)$$

The Bejan number can be written in the context of thermodynamics as follows:

$$Be = \frac{\dot{S}'_{gen,heat\,transfer}}{\dot{S}'_{gen,heat\,transfer} + \dot{S}'_{gen,\,fluid\,\,friction}} \tag{17}$$

The Bejan number is defined as the ratio of heat transfer irreversibility to total irreversibility due to heat transfer and fluid friction.

4. NUMERICAL METHOD

The simulations are conducted with Finite Volume Method (FVM). In the coupling of pressure and velocity terms, Semi-Implicit Method for Pressure Linked Equation (SIMPLE) algorithm is applied [40]. To discretize the convection and diffusion terms, second order upwind scheme is utilized. The residual convergence criterion is selected 10^{-6} in numerical tests for governing equations.

Hexagonal meshes are used in the modeling of minichannel. To obtain detailed and accurate results for boundary layer, finer meshes are used in the regions close to minichannel walls and corners. For mesh independency test, the different mesh numbers are used. As a consequence of grid independency test, the mesh structure consisting of 30 nodes on width, 50 nodes on height and 500 nodes of length is selected as the best mesh structure.

5. ARTIFICIAL NEURAL NETWORK

Artificial Neural Network consisting of inputs by users and an output reflecting the information kept in connections during training is a nonlinear system involving neurons and weighted connection links. A multilayer artificial neural network involves at least three layer, namely, input, hidden and output layers demonstrated in Fig. 1. The referred learning or training is reached by decreasing the sum of square error between the predicted output of ANN and the actual output from training data, by continuously adjusting and lastly defining the weights that connects neurons in conjunctive layers.

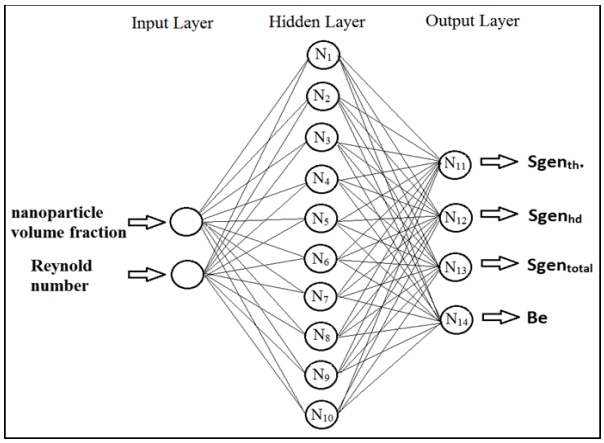

Figure 1. Artificial neural network structure

ANN analyses are performed for $\dot{S}'_{gen,th}$, $\dot{S}'_{gen,hd}$, $\dot{S}'_{gen,total}$ and Be values in 50 numerical results that are 10 results for nanoparticle volume fraction. Reynold number and nanoparticle volume fraction are entered as independent parameters (inputs) and $\dot{S}'_{gen,th}$, $\dot{S}'_{gen,hd}$, $\dot{S}'_{gen,total}$ and Be values are entered as dependent parameter (output) in ANN software program. 10 numerical results are chosen for testing (confirmation) and rest of 40 results are used as training data in MATLAB software program. The most appropriate topology is determined as 2-10-4 after many trial-errors with ANN (Fig.1). It is stated that Levenberg–Marquardt algorithm is used due to the fastest method and one level hidden layer with 10 neurons has been chosen. As a result, N1, N2, N3, N4, N5, N6, N7, N8, N9, N10 and N11, N12, N13, N14 neurons are determined as hidden layer and output layer, respectively.

The weights of each neurons have been specified in training result and average deviation value has been calculated from ANN output values and experimental results. Output neurons developed for estimated $\dot{S}'_{gen,th}$, $\dot{S}'_{gen,hd}$, $\dot{S}'_{gen,total}$ and Be have been calculated by using Fermi transfer function.

$$E_{i11-14} = \frac{1}{1+e^{-4\left(\sum_i^n w_i N_i - 0.5\right)}} \tag{18}$$

Here, n and w_i show the number of neurons used in hidden layer and weights of neurons, respectively. N_i is the effect on $\dot{S}'_{gen,th}$, $\dot{S}'_{gen,hd}$, $\dot{S}'_{gen,total}$ and Be of each neuron used in hidden layer. According to input parameters in ANN model;

$$E_i = 4\left(c_{1i}VF + c_{2i}\,Re - 0.5\right) \tag{19}$$

$$N_i = \frac{1}{1+e^{-E_i}} \tag{20}$$

are defined. C_{ij} constants show the weight of each neuron used in hidden layer after the result of data training set in MATLAB software. While C_{ij} values have 10 constants in hidden layer those have been given in Table 1.

Table 1. Weights of each neurons for $\dot{S}'_{gen,th}$, $\dot{S}'_{gen,hd}$, $\dot{S}'_{gen,total}$ and Be

i	***C1i***	***C2i***
1	3.2023	1.2084
2	1.6103	3.2745
3	0.25359	-2.0317
4	-4.0298	1.6172
5	-4.5109	1.215
6	1.6045	1.7605
7	-4.0538	1.7741
8	-2.9469	-2.4593
9	4.0887	1.6186
10	2.1825	4.3813

5.1. K-Fold Cross validation

Cross-validation is a measurement of assessing the performance of a predictive model, and statistical analysis will generalize to an independent dataset. There are many types of cross-validation, such as repeated random sub-sampling validation, K-fold cross validation (Figure 2), K x 2 cross-validations, leave-one-out cross-validation and so on (Figure 3).

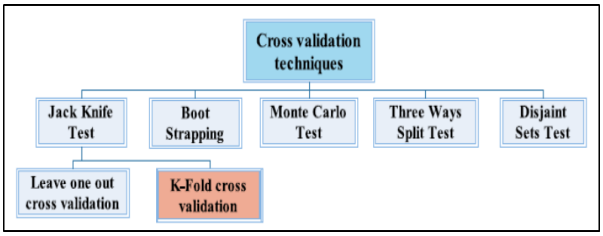

Figure 2. Diagram of cross validation techniques types [41].

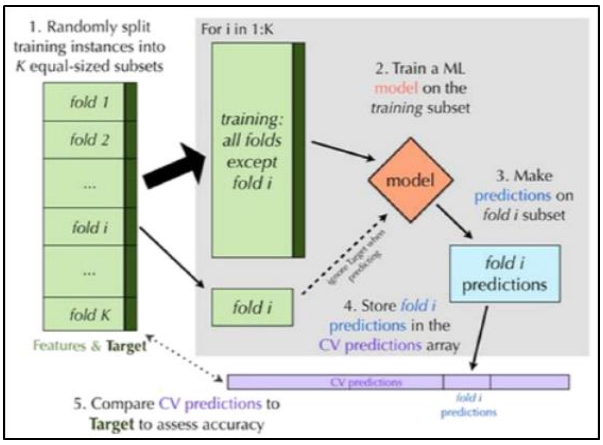

Figure 3. Flowchart of the K-fold cross-validation [41].

In this study, we pick up 5-fold cross-validation for selecting parameters of model. The K-fold cross-validation is a technique of dividing the original sample randomly into K subsamples. Then, a single sub-sample is regarded as the validation data for testing the model, and the remaining K-1 sub-samples are used as training data. These processes are repeated K times and each of the K sub-samples used exactly one as the validation data. The K results from the folds can then be averaged (or otherwise combined) to produce a single estimation. The ANN model (test results) showed in this study has the lowest error among 5 subsamples.

5.2. Performance evaluation criteria

In the final stage of this study, reliability of mathematical model is assessed with various error control methods in order to demonstrate the suitability of model. Due to fact that training and testing procedure in ANN is performed by considering an error value (e), average of the sum of these error values is needed to be minimized. This minimized value is the mean squared error (MSE) that is a criteria determining the ANN performance. Root-mean-squared (RMS), coefficient of determination (R^2), mean absolute percentage error (MAPE) has been taken into consideration as criteria in similarity between experimental and ANN results.

$$MSE = \frac{1}{p}\sum_i e_i^2 = \frac{1}{p}\sum_i (t_i - o_i)^2 \quad (21)$$

$$RMS = \sqrt{MSE} = \sqrt{\frac{1}{p}\sum_i e_i^2} = \sqrt{\frac{1}{p}\sum_i (t_i - o_i)^2} \quad (22)$$

$$R^2 = 1 - \left(\frac{\sum_i (t_i - o_i)^2}{\sum_i o_i^2} \right) \quad (23)$$

$$MAPE = \frac{1}{p}\sum_i \left(\frac{|t_i - o_i|}{t_i} \right) \times 100 \quad (24)$$

In Eqs. 21-24, p, t_i, o_i and e_i show the sample simulation number, output value from simulations, output value from ANN and error value, respectively. The applicability of developed model increases when R^2 value approaches to 1.

6. RESULTS and DISCUSSION

The convective heat transfer and entropy generation of Ag-MgO/water hybrid nanofluid flow through rectangular minichannel are numerically investigated for different Reynolds number and nanoparticle volume fractions. The flow is considered as laminar flow and the Reynolds number is in the range of 200 and 2000. The nanoparticle volume fraction (ϕ) of Ag-MgO/water hybrid nanofluid is varied between 0.005 and 0.02. Constant heat flux of 100 W/m^2 is applied at the bottom surface of minichannel.

The variation of convective heat transfer coefficient of Ag-MgO/water hybrid nanofluid with the Reynolds number for different nanoparticle volume fractions is shown in Fig. 4.

As can be seen from Fig. 4., the convective heat transfer coefficient of Ag-MgO/water hybrid nanofluid flow increases with increase in both the Reynolds number and nanoparticle volume fraction. The maximum convective heat transfer coefficients are obtained for Ag-MgO/water hybrid nanofluid having nanoparticle volume fraction of ϕ=0.02 at Re=2000. At Re=2000, the convective heat transfer coefficient obtained for ϕ=0.02 Ag-MgO/water hybrid nanofluid is 21.29% higher compared to that of pure water.

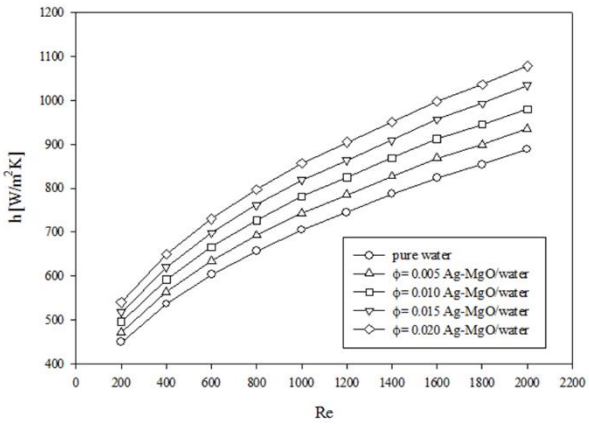

Figure 4. Convective heat transfer coefficient

As can be seen from Fig. 4., the convective heat transfer coefficient of Ag-MgO/water hybrid nanofluid flow increases with increase in both the Reynolds number and nanoparticle volume fraction. The maximum convective heat transfer coefficients are obtained for Ag-MgO/water hybrid nanofluid having nanoparticle volume fraction of ϕ =0.02 at Re=2000. At Re=2000, the convective heat transfer coefficient obtained for ϕ =0.02 Ag-MgO/water hybrid nanofluid is 21.29% higher compared to that of pure water.

The change of Nusselt number of Ag-MgO/water hybrid nanofluid with the Reynolds number for different nanoparticle volume fractions is illustrated in Fig. 5.

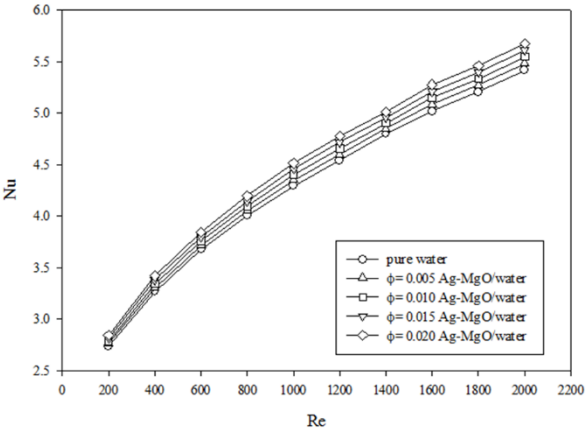

Figure 5. The Nusselt number

It is clear that the Nusselt number of Ag-MgO/water hybrid nanofluid flow increases with increasing in both the Reynolds number and nanoparticle volume fraction. The Nusselt number values obtained for ϕ =0.02 Ag-MgO/water hybrid nanofluid at Re=200 and at Re=2000 are Nu=2.84 and Nu=5.68, respectively. At Re=2000, the Nusselt number value for ϕ =0.02 Ag-MgO/water hybrid nanofluid is 4.76% higher than that of pure water. The lower enhancement in the Nusselt number compared to pure water is due to the fact that the nanoparticle addition to working fluid simultaneously increases the convective and conductive heat transfer coefficients. For this study, higher increment obtained for convective heat transfer coefficient compared to conductive heat transfer caused to increment in the Nusselt number.

The variation of Darcy friction factor of Ag-MgO/water hybrid nanofluid with the Reynolds number for different nanoparticle volume fractions is illustrated in Fig. 6.

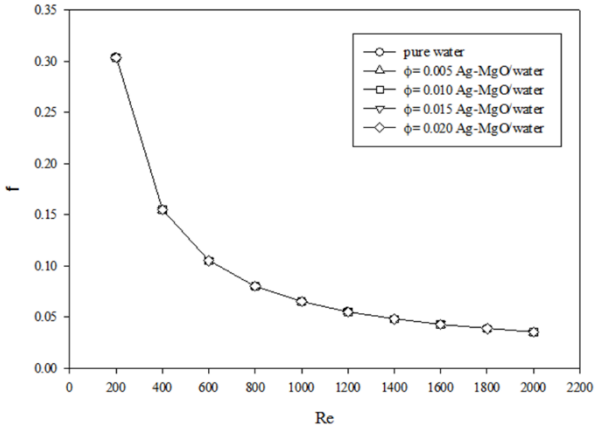

Figure 6. The Darcy friction factor

The Darcy friction factor of Ag-MgO/water hybrid nanofluid decreases with increasing the Reynolds number. However, it is not affected by nanoparticle volume fraction. Nanoparticle addition to working fluid causes to an increment in pressure drop; however, does not affect dimensionless pressure drop. Therefore, the Darcy friction factor does not change for different nanoparticle volume fractions.

The change of entropy generation due to heat transfer per unit length of Ag-MgO/water hybrid nanofluid with the Reynolds number for different nanoparticle volume fractions is illustrated in Fig. 7.

As can be seen from Fig. 7, the entropy generation due to heat transfer per unit length decreases with decrease in both the Reynolds number and nanoparticle volume fraction. At Re=2000, the entropy generation due to heat transfer per unit length obtained for ϕ =0.02 Ag-MgO/water hybrid nanofluid is 1.18×10^{-6} W/mK, while it is 1.44×10^{-6} W/mK for pure water at same Reynolds number value. The reason of reduction in entropy generation due to heat transfer arising from nanoparticle addition is that convective heat transfer coefficient increases with increase in nanoparticle volume fraction.

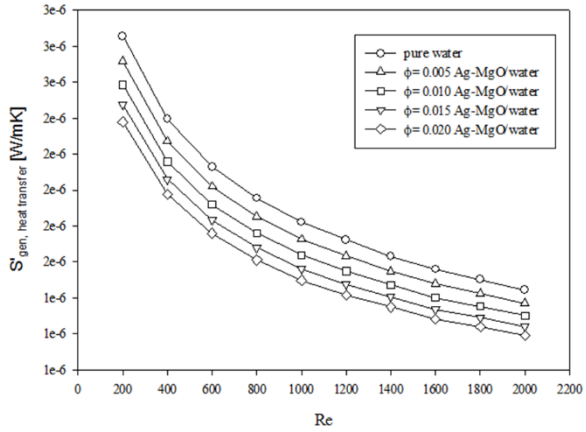

Figure 7. Entropy generation due to heat transfer per unit length

The variation of entropy generation due to fluid friction per unit length of Ag-MgO/water hybrid nanofluid with the Reynolds number for different nanoparticle volume fractions is shown in Fig. 8.

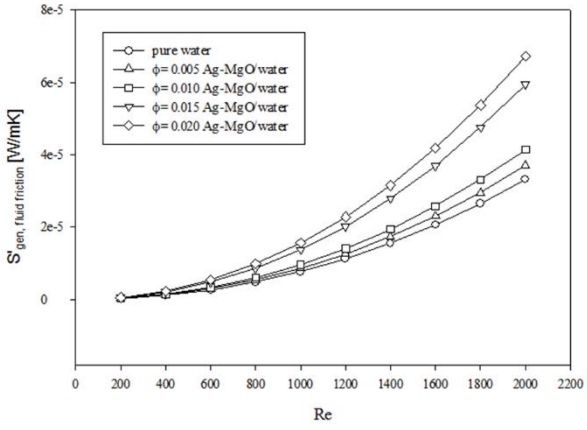

Figure 8. Entropy generation due to fluid friction per unit length

The entropy generation due to fluid friction per unit length of Ag-MgO/water hybrid nanofluid increases with increase in both the Reynolds number and nanoparticle volume fraction. The highest entropy generation values due to fluid friction per unit length are obtained for ϕ =0.02 Ag-MgO/water hybrid nanofluid. At Re=2000, the entropy generation value due to fluid friction for pure water is 3.31×10^{-5} W/mK, while it is 6.73×10^{-5} W/mK for ϕ =0.02 Ag-MgO/water hybrid nanofluid. For this study, the analyses are realized for fixed Reynolds numbers. To obtain the defined Reynolds number, the velocity value of flow increases with nanoparticle addition to working fluid. In addition, the density and bulk temperature of flow increases with increase in nanoparticle volume fraction of Ag-MgO/water hybrid nanofluid. These increments in velocity and density and decrement in bulk temperature of the flow with nanoparticle addition cause to increase in entropy generation due to fluid friction of flow.

The variation of total entropy generation per unit length of Ag-MgO/water hybrid nanofluid with the Reynolds number for different nanoparticle volume fractions is shown in Fig. 9.

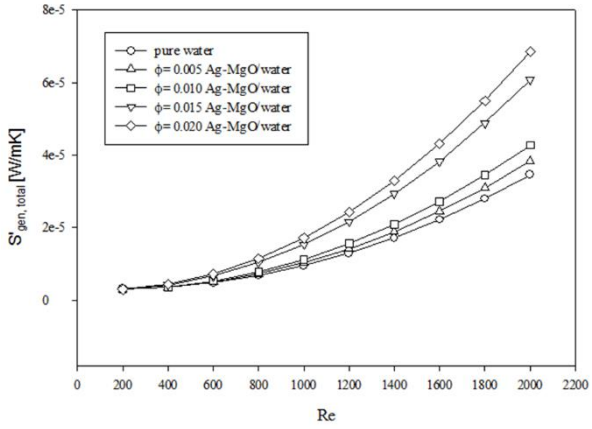

Figure 9. Total entropy generation per unit length

As can be seen from Fig. 9, the total entropy generation increases with increase in both the Reynolds number and nanoparticle volume fraction. The results obtained for total entropy generation and for entropy generation due to fluid friction are almost same. This situation shows that the fluid friction is dominant factor for total entropy generation of flow. This is due to that the minichannel considered in this study has very small hydraulic diameter.

The variation of the Bejan number of Ag-MgO/water hybrid nanofluid with the Reynolds number for different nanoparticle volume fractions is illustrated in Fig. 10.

As expected, the Bejan number of Ag-MgO/water hybrid nanofluid flow decreases with increase both in the Reynolds number and nanoparticle volume fraction. Bejan number expresses the domination of heat transfer on the total entropy generation of flow. As mentioned above, the entropy generation due to fluid friction is dominant for this study, and it increases with increase in nanoparticle volume fraction. Therefore, the Bejan number decreases with increasing nanoparticle volume fraction. At Re=200, the Bejan number values obtained for pure water and ϕ =0.02 Ag-MgO/water hybrid nanofluid are 0.9085 and 0.8028, respectively. Whereas, at Re=2000, pure water and ϕ =0.02 Ag-MgO/water hybrid nanofluid has a Bejan number of 0.0417 and 0.0174, respectively.

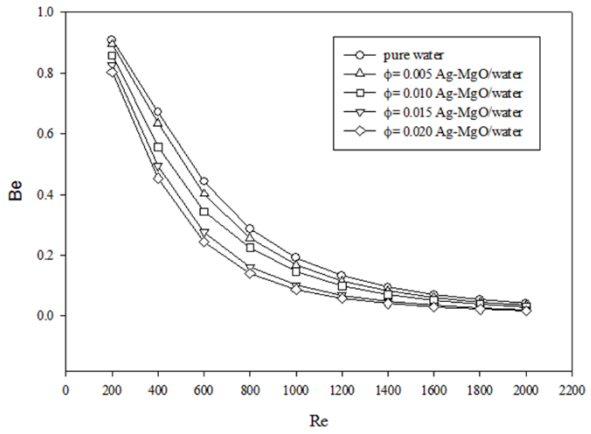

Figure 10. The Bejan number

In this study, 5-fold cross validation was performed and the test results having the lowest error were used for this ANN analysis. Table 2-5 shows that mean absolute percentage errors for $\dot{S}'_{gen,th}$, $\dot{S}'_{gen,hd}$, $\dot{S}'_{gen,total}$ and Be have been calculated as 0.80013, 4.08908, 2.48949, 4.253272% in training results while it is 1.38476, 7.41604, 2.54823, 8.595395 % in testing results. The calculation of all R^2 values above 99% shows the higher reliability of ANN model for $\dot{S}'_{gen,th}$, $\dot{S}'_{gen,hd}$, $\dot{S}'_{gen,total}$ and Be. The comparison of $\dot{S}'_{gen,th}$, $\dot{S}'_{gen,hd}$, $\dot{S}'_{gen,total}$ and Be obtained from experimental and ANN results has been illustrated in Fig. 11-14. It is clearly seen that the output values for both experimental and ANN are very close to each other. In addition, it is confirmed that this ANN model is high accurate and applicable in future studies.

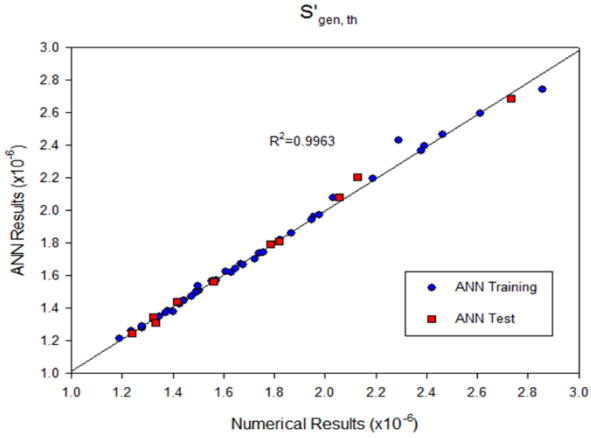

Figure 11. ANN performance for $\dot{S}'_{gen,th}$

Table 2. The statistical error values for $\dot{S}'_{gen,th}$

	RMS	***MSE***	***R²***	***MAPE***
ANN Training Data	0,03227	0,00104	0,99967	0,80013
ANN Test Data	0,03289	0,00108	0,99967	1,38476
ANN- Total	0,95763	0,91706	0,99967	0,91706

Table 3. The statistical error values for $\dot{S}'_{gen,hd}$

	RMS	***MSE***	***R²***	***MAPE***
ANN Training Data	0,92758	0,860404	0,99846	4,08908
ANN Test Data	1,44230	2,0802	0,99670	7,41604
ANN- Total	2,18048	4,7545	0,99807	4,75447

Table 4. The statistical error values for $\dot{S}'_{gen,total}$

	RMS	***MSE***	***R²***	***MAPE***
ANN Training Data	0,83922	0,7043	0,99886	2,48949
ANN Test Data	1,16831	1,36495	0,99829	2,54823
ANN- Total	1,58153	2,50124	0,99872	2,50124

Table 5. The statistical error values for Be

	RMS	***MSE***	***R²***	***MAPE***
ANN Training Data	0,014537	0,000211	0,998354	4,253272
ANN Test Data	0,016840	0,000284	0,997970	8,595395
ANN- Total	2,263117	5,1217	0,998272	5,121697

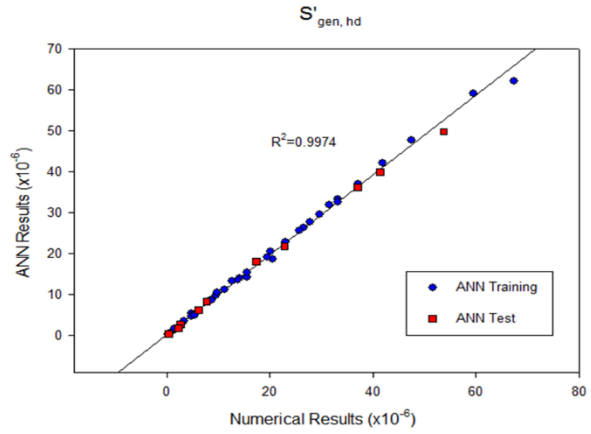

Figure 12. ANN performance for $\dot{S}'_{gen,hd}$

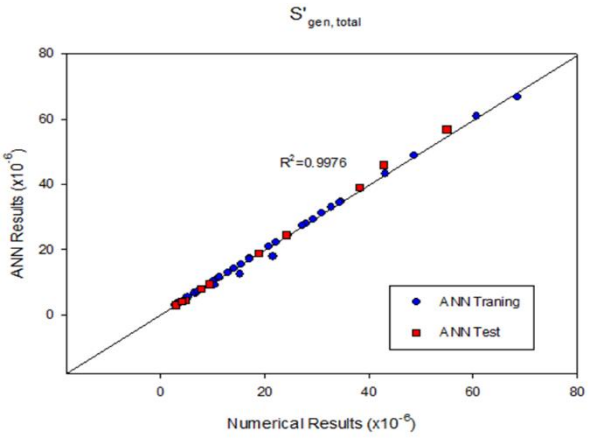

Figure 13. ANN performance for $\dot{S}'_{gen,total}$

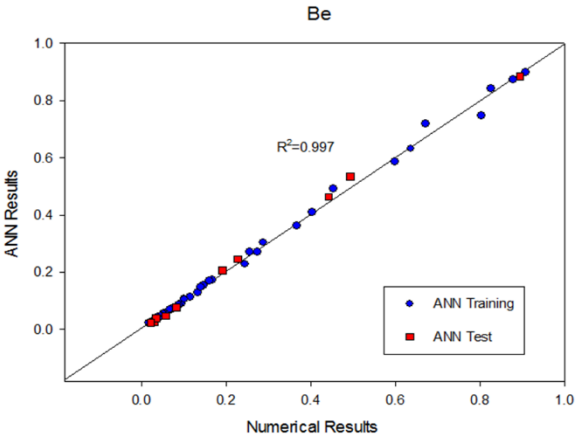

Figure 14. ANN performance for *Be* .

7. CONCLUSIONS

In this study, convective heat transfer and entropy generation of Ag-MgO/water hybrid nanofluid flow through rectangular minichannel were numerically investigated. A constant heat flux was applied to the bottom wall of minichannel and flow was considered under laminar flow conditions. The Reynolds number ranged between Re=200 and Re=2000 and nanoparticle volume fraction was in the range of ϕ =0.005 and 0.02. Results showed that the convective heat transfer enhancement is obtained with Ag-MgO hybrid nanoparticle addition to pure water. Increase in nanoparticle volume fraction of Ag-MgO hybrid nanoparticle caused to decrease in entropy generation due to heat transfer; however, caused to increase in entropy generation due to fluid friction. For this study, it was observed that the fluid friction is dominant parameter in the total entropy generation. It is due to that the minichannel considered in this study has a very small hydraulic diameter. In this study, an ANN model was created to estimate the entropy generation of Ag-MgO hybrid nanofluid. The results obtained by ANN model showed good agreement with the numerical results. It was confirmed that this ANN model has high accuracy for estimation of entropy generation and applicable in future studies.

REFERENCES

[1] Maxwell J.C., "A Treatise on Electricity and Magnetism", 2nd ed., ***Clarendon Press Series***, Oxford, (1873).

[2] Choi S.U.S. and Eastman J.A., "Enhancing thermal conductivity of fluids with nanoparticles", ***ASME International Mechanical Engineering Congress and Exposition***, San Francisco, 1-8, (1995).

[3] Bobbo S., Fedele L., Benetti A., Colla L., Fabrizio M., Pagura C. and Barison S., "Viscosity of water based SWCNH and TiO_2 nanofluids", ***Experimental Thermal and Fluid Science***, 36: 65-71, (2012).

[4] Wang W., Xu X. and Choi S.U.S., "Thermal conductivity of nanoparticle-fluid mixture", ***Journal of Thermophysics and Heat Transfer***, 13: 474-480, (1999).

[5] Nguyen C.T., Desgranges F., Galanis N., Roy G., Mare T., Boucher S. and Mintsa H.A., "Viscosity data for Al2O3-water nanofluid-hysteresis: is heat transfer enhancement using nanofluids reliable?", ***International Journal of Thermal Sciences***, 47: 103-111, (2008).

[6] Pak B.C. and Cho Y.I., "Hydrodynamic and heat transfer study of dispersed fluids with submicron metallic oxide particles", ***Experimental Heat Transfer***, 11: 151-170, (1998).

[7] Chandrasekar M., Suresh S. and Bose A.C, "Experimental investigations and theoretical determination of thermal conductivity and viscosity of Al_2O_3/water nanofluid", ***Experimental Thermal and Fluid Science***, 34: 210-216, (2010).

[8] Masuda H., Ebata A., Teramae K. and Hishinuma N., "Alteration of thermal conductivity and viscosity of liquid by dispersing ultra-fine particles. Dispersion of Al_2O_3, SiO_2 and TiO_2 ultra-fine particles", ***Netsu Bussei***, 7: 227-233, (1993).

[9] Turgut A., Tavman I., Chirtoc M., Schuchmann H.P., Sauter C. and Tavman S., "Thermal conductivity and viscosity measurements of water-based TiO2 nanofluid", ***International Journal of Thermophysics***, 30: 1213-1226, (2009).

[10] Li C.H. and Peterson G.P., "Experimental investigation of temperature and volume fraction variations on the

effective thermal conductivity of nanoparticle suspensions (nanofluids)", ***Journal of Applied Physics***, 99: 084314 1-8 (2006).

[11] Kang H.U., Kim S.H. and Oh J.M., "Estimation of thermal conductivity of nanofluid using experimental effective particle volume", ***Experimental Heat Transfer***, 19: 181-191 (2006).

[12] F. Qiao, "Preparation and property Ag, Graphene nanofluids", ***Master Dissertations***, Qingdao University of Science and Technology, (2010).

[13] Sharma P., Baek I.H., Cho T., Park S. and Lee K.B., "Enhancement of thermal conductivity of ethylene glycol based silver nanofluids", ***Powder Technology***, 208: 7-19, (2011).

[14] Jung J.-Y., Oh H.-S. and Kwak H.-Y., "Forced convective heat transfer of nanofluids in microchannels", ***International Journal of Heat and Mass Transfer***, 52: 466-472, (2009).

[15] Haghighi E.B., Utomo A.T., Ghanbarpour M., Zavareh A.I.T., Poth H., Khodabandeh R., Pacek A. and B.E. Palm, "Experimental study on convective heat transfer of nanofluids in turbulent flow: Methods of comparison of their performance", ***Experimental Thermal and Fluid Science***, 57: 378-387, (2014).

[16] Mirfendereski S., Abbassi A., Saffar-avval M., "Experimental and numerical investigation of nanofluid heat transfer in helically coiled tubes at constant wall heat flux", ***Advanced Powder Technology***, 26: 1483-1494, (2015).

[17] Allahyar H.R., Hormozi F. and ZareNezhad B., "Experimental investigation on the thermal performance of a coiled heat exchanger using a new hybrid nanofluid", ***Experimental Thermal and Fluid Science***, 76: 324-329, (2016).

[18] Yu J., Kang S.-W., Jeong R.-G. and Banerjee D., "Experimental validation of numerical predictions for forced convective heat transfer of nanofluids in a microchannel", ***International Journal of Heat and Fluid Flow***, 62: 203-212, (2016).

[19] Selvam C., Irshad E.C.M., Lal D.M. and Harish S., "Convective heat transfer characteristics of water-ethylene glycol mixture with silver nanoparticles", ***Experimental Thermal and Fluid Science***, 77: 188-196, (2016).

[20] Bourantas G.C., Skouras E.D., Loukopoulos V.C. and Burganos V.N., "Heat transfer and natural convection of nanofluids in porous media", ***European Journal of Mechanics-B/Fluids***, 43: 45-56, (2014).

[21] Sundar L.S., Singh M.K. and Sousa A.C.M., "Enhanced heat transfer and friction factor of MWCNT-Fe_3O_4/water hybrid nanofluids", ***International Communications in Heat and Mass Transfer***, 52: 73-83, (2014).

[22] Suresh S., Venkitaraj K.P., Selvakumar P. and Chandrasekar M., "Effect of Al2O3-Cu/water hybrid nanofluid in heat transfer", ***Experimental Thermal and Fluid Science***, 38: 54-60, (2012).

[23] Ahmad U.K., Hasreen M., Yahaya N.A. and Rosnadiah B., "Comparative study of heat transfer and friction factor characteristics of nanofluids in rectangular channel", ***Procedia Engineering***, 170: 541-546, (2017).

[24] Babu J.A.R., Kumar K.K. and Rao SS., "State-of-art review on hybrid nanofluids", ***Renewable and Sustainable Energy Reviews***, 77: 551-565 (2017).

[25] Atashrouz S., Pazuki G. and Alimoradi Y., "Estimation of the viscosity of nine nanofluids using a hybrid GMDH-type neural network system", ***Fluid Phase Equilibra***, 372: 43-48 (2014).

[26] Longo G.A., Zilio C., Ortombina L. and Zigliotto M., "Application of artificial neural network (ANN) for modeling oxide-based nanofluids dynamic viscosity", ***International Communications in Heat and Mass Transfer***, 83: 8-14 (2017).

[27] Longo G.A., Zilio C., Ceseracciu E. and Reggiani M., "Application of artificial neural network (ANN) for the prediction of thermal conductivity of oxide-water nanofluids", ***Nano Energy***, 1: 290-296, (2012).

[28] Esfe M. H., Saedodin S., Sina N., Afrand M. and Rostami S., "Designing an artificial neural network to predict thermal conductivity and dynamic viscosity of ferromagnetic nanofluid", ***International Communications in Heat and Mass Transfer***, 68: 50-57, (2015).

[29] Esfe M. H., Wongwises S., Naderi A., Asadi A., Safaei M. R., Rostamin H., Dahari M. and Karimipour A., "Thermal conductivity of Cu/TiO_2-water/EG hybrid nanofluid: Experimental data and modeling using artificial neural network and correlation", ***International Communications in Heat and Mass Transfer***, 66: 100-104, (2015).

[30] Santra A. K., Chakraborty N. and Sen S., "Prediction of heat transfer due to presence of copper-water nanofluid using resilient-propagation neural network", ***International Journal of Thermal Sciences***, 48: 1311-1318, (2009).

[31] Tafarroj M. M., Mahian O., Kasaeian A., Sakamatapan K., Dalkilic A. S. and Wongwises S., "Artificial neural network modeling of nanofluid flow in a microchannel heat sink using experimental data", ***International Communications in Heat and Mass Transfer***, 86: 25-31, (2017).

[32] Ghahdarijani A. M., Hormozi F. and Asl A. H., "Convective heat transfer and pressure drop study on nanofluids in double-walled reactor by developing an optimal multilayer perceptron artificial neural network", ***International Communications in Heat and Mass Transfer***, 84: 11-19, (2017).

[33] Safikhani H., Abbassi A., Khalkhali A. and Kalteh M., "Multi-objective optimization of nanofluid flow in flat tubes using CFD, Artificial Neural Networks and genetic algorithms", ***Advanced Powder Technology***, 25: 1608-1617, (2014).

[34] Tomy A. M., Ahammed N., Subathra M. S. P. and Asirvatham L. G., "Analysing the performance of a flat plate solar collector with silver/water nanofluid using artificial neural network", ***Procedia Computer Science***, 93: 33-40, (2016).

[35] Bahiraei M. and Majd S. M., "Prediction of entropy generation for nanofluid flow through a triangular minichannel using neural network", ***Advanced Powder Technology***, 27: 673-683, (2016).

[36] Kandlikar S., Garimella S., Li D., Colin S. and King M. R., "Heat Transfer and Fluid Flow in Minichannels and

Microchannels", ***Elsevier Science and Technology***, (2005).

[37] Das S. K., Choi S. U. S., Yu W. and Pradeep T., "Nanofluids: Science and Technology", ***John Wiley & Sons***, Jersey, (2008).

[38] Esfe M. H., Arani A. A. A., Rezaie M., Yan W.-M. and Karimipour A., "Experimental determination of thermal conductivity and dynamic viscosity of Ag-MgO/water hybrid nanofluid", ***International Communications in Heat and Mass Transfer***, 66: 189-195, (2015).

[39] Bejan A., "Entropy Generation through Heat and Fluid Flow", ***John Wiley and Sons***, 1982.

[40] Patankar S. V., "Numerical Heat Transfer and Fluid Flow", ***CRC Press***, (1980).

[41] Rohani A., Taki M. and Abdollahpour M., "A novel soft computing model (Gaussian process regression with K-fold cross validation) for daily and monthly solar radiation forecasting (Part: I)", ***Renewable Energy***, 115: 411-422, (2018).